Response of biogenic secondary organic aerosol formation to anthropogenic NOx emission mitigation

Zhizhao Wang, Florian Couvidat, Karine Sartelet

Science of the Total Environment 927 (2024) 172142

Contents lists available at ScienceDirect

Science of the Total Environment

journal homepage: www.elsevier.com/locate/scitotenv

Response of biogenic secondary organic aerosol formation to anthropogenic NOx emission mitigation

Zhizhao Wang [a,b,c,d,*], Florian Couvidat [b], Karine Sartelet [a]

[a] Centre d'Enseignement et de Recherche en Environnement Atmosphérique (CEREA), Ecole des Ponts ParisTech, EdF R&D, IPSL, Marne-la-Vallée 77455, Île-de-France, France
[b] Institut National de l'Environnement Industriel et des Risques (INERIS), Verneuil-en-Halatte, 60550 Oise, France
[c] Now at University of California, Riverside (UCR), Riverside 92521, CA, USA
[d] Now at National Center for Atmospheric Research (NCAR), Boulder 80301, CO, USA

HIGHLIGHTS

- Comparison of simulations with SOA mechanisms of different complexity: GBM vs. H^2O
- GBM outperforms H^2O in matching observed aerosol data.
- Biogenic SOA increase from NOx mitigation if detailed SOA mechanisms are used.
- 3-D simulations require detailed SOA mechanisms for accurate SOA responses.

GRAPHICAL ABSTRACT

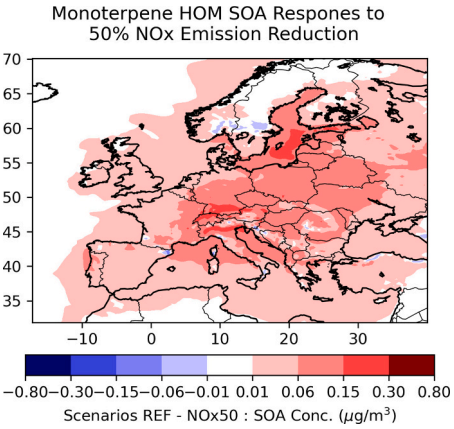

ARTICLE INFO

Editor: Hai Guo

Keywords:
Aerosol mechanism
NOx emission reduction
Monoterpene SOA mechanism
Sesquiterpene SOA mechanism
Chemical transport modeling

ABSTRACT

This study investigates the effects of anthropogenic nitrogen oxide (NOx) mitigation reduction on secondary organic aerosol (SOA) formation from monoterpene and sesquiterpene precursors across Europe, using the three-dimensional (3-D) Chemical Transport Model (CTM) CHIMERE.

Two SOA mechanisms of varying complexity are employed: the GENOA-generated Biogenic Mechanism (GBM) and the Hydrophobic/Hydrophilic Organic mechanism (H^2O). GBM is a condensed SOA mechanism generated by automatic reduction from near-explicit chemical mechanisms (i.e., the Master Chemical Mechanism - MCM and the peroxy radical autoxidation mechanism - PRAM) using the GENerator of Reduced Organic Aerosol Mechanisms version 2.0 (GENOA v2.0). Conversely, the H^2O mechanism is developed primarily based on experimental data, with simplified chemical pathways and SOA formation yields reflecting those from chamber experiments.

* Corresponding author at: Centre d'Enseignement et de Recherche en Environnement Atmosphérique (CEREA), Ecole des Ponts ParisTech, EdF R&D, IPSL, Marne-la-Vallée, 77455 Île-de-France, France.
E-mail address: zhizhaow@ucr.edu (Z. Wang).

https://doi.org/10.1016/j.scitotenv.2024.172142
Received 19 December 2023; Received in revised form 21 March 2024; Accepted 30 March 2024
Available online 6 April 2024

In the 3-D simulations conducted for the summer of 2018 over Europe, the implementation of GBM significantly improved the model's performance in comparison to simulations using the H^2O mechanism, yielding results more consistent with measured aerosol concentrations extracted from the EBAS database.

In response to NOx emission mitigation, simulated SOA concentrations increase with GBM but decrease when using the H^2O mechanism, unless a highly oxygenated molecules (HOMs) formation scheme is incorporated. The SOA composition becomes more oxidized and concentrations elevate after NOx reduction, particularly in simulations using GBM. These higher concentrations are likely due to enhanced reaction rates of organic peroxy radicals (RO_2) with HO_2, resulting in more oxidized products from monoterpene degradation that favors HOM formation. The results suggest that detailed SOA mechanisms including autoxidation are necessary for accurate predictions of SOA concentrations in 3-D modeling.

1. Introduction

Atmospheric aerosols significantly impact air quality, climate, and human health (Breysse et al. (2013); Seinfeld et al. (2016); McNeill (2017)). Among various aerosol types, secondary organic aerosols (SOAs) have received much attention in air quality studies (e.g., Kanakidou et al. (2005); Hallquist et al. (2009); Couvidat et al. (2013); Huang et al. (2014)). The processes governing SOA formation in the atmosphere are intricate, involving multiphase physicochemical transformations, and remain a subject of ongoing investigation. (Hodzic et al. (2016)). The major pathway for SOA formation is through the gas-particle mass transfer of low-volatility oxidation products formed from the oxidation of volatile organic compounds (VOCs) upon their release into the troposphere (Hallquist et al. (2009)). As SOAs are formed, the chemical aging of aerosols, which results from successive oxidation steps beyond the initial generations, is often enhanced by multi-generation gas-phase oxidations (Donahue et al. (2006); Wang et al. (2018)). Due to the diverse origins of VOCs and varying atmospheric conditions, SOA composition and concentrations exhibit spatial and temporal variations.

Generally, VOCs originate from numerous sources, including biogenic emissions from vegetation, anthropogenic emissions from human activities such as transportation, manufacturing, and consumer care products, as well as biomass burning. Guenther et al. (2012) reported an annual production of approximately 1000 Tg of biogenic VOCs, with 50 % from isoprene, 15 % from monoterpenes, and 3 % from sesquiterpenes. Although the emissions of monoterpene and sesquiterpene are lower than those of isoprene, they strongly influence SOA formation because of their higher yields (Seigneur (2019)).

In contrast to biogenic VOCs, anthropogenic VOCs are linked directly to human activity. Besides VOCs, anthropogenic emissions also include a range of other pollutants, such as nitrogen oxides (NOx) and sulfur dioxide (SO_2), which can alter aerosol formation (Xu et al. (2021)). Particularly, NOx is among the most significant anthropogenic pollutants affecting SOA formation (Ng et al. (2007); Porter et al. (2021)). In addition to its crucial role in the formation and destruction of tropospheric ozone, which subsequently alters the oxidation pathways of SOA precursors, NOx also directly reacts with the organic peroxy radicals (RO_2) formed by the oxidation of precursors and therefore affects the chemical regime of SOA formation.

Current regulation efforts, such as those targeting traffic, are leading to significant reductions in NOx emissions (André et al. (2020)). Traditionally, it has been considered that biogenic organic aerosol concentrations tend to decrease in response to current emission regulations and the reduction of anthropogenic emissions, particularly in rural and peri-urban areas where oxidant concentrations (e.g., ozone) are predicted to decrease (Sartelet et al. (2012); Shrivastava et al. (2019)). However, recent studies suggested that reducing anthropogenic emissions could potentially lead to less significant reductions in organic aerosol concentrations or even an increase in some cases (Huang et al. (2020); Li et al. (2024)). These non-linear effects could be attributed to a shift between low-NOx and high-NOx conditions or even to complex interactions among products formed from individual VOCs (Takeuchi et al. (2022)). This highlights the need for further investigation into the influences of emission reduction on SOA formation. To effectively mitigate the impact of anthropogenic emissions on the environment, it is necessary to accurately predict the influences of those emissions on aerosol formation. This requires a comprehensive understanding of accurate VOC chemistry, accounting for the interactions between emissions and aerosol formation, and considering the influences of environmental conditions and atmospheric pollutants.

Explicit chemical mechanisms integrate our up-to-date knowledge of VOC chemistry derived from theoretical and experimental studies. These mechanisms include the Generator for Explicit Chemistry and Kinetics of Organics in the Atmosphere (GECKO-A; Aumont et al. (2012)), the Statewide Air Pollution Research Center (SAPRC) mechanism generation system (MechGen; Carter et al. (2023)) - both are fully explicit - and the near-explicit Master Chemical Mechanism (MCM; Jenkin et al. (1997)), which lumps reactions after first and second generations. In a development closely aligned with MCM, the Peroxy Radical Autoxidation Mechanism (PRAM) addresses RO_2 autoxidation and the formation of extremely low-volatility organic compounds (ELVOCs) from monoterpenes (Roldin et al. (2019)). Those highly oxygenated organic molecules (HOMs) have garnered significant attention in the last decade due to their potentially high contribution to SOA formation, with reported yields ranging from 0.1 % to 17 % (Bianchi et al. (2019)), and modeling estimates suggesting they could account for up to 50 % of monoterpene SOAs (Roldin et al. (2019)). Studies have also highlighted the enhanced HOM formation under low-NOx conditions (e.g., Ehn et al. (2014)), as elevated NOx can efficiently terminate RO_2 autoxidation, thereby reducing HOM yields (Wang et al. (2023a)).

However, the direct application of these explicit or near-explicit chemical mechanisms in large-scale modeling is often limited due to computational constraints (Li et al. (2015)). To be computationally efficient, Three-dimensional (3-D) Chemistry-Transport Models (CTM) typically employ simplified chemical mechanisms that rely on a limited set of model species and reactions to simulate organic aerosol formation. These simplified mechanisms are usually built from chamber measurements. The most widely used approaches for deriving these simplified mechanisms of SOA formation include the two-product Odum approach (Odum et al. (1996)), the volatility basis set (VBS) approach (Donahue et al. (2006)), and the surrogate approach (e.g., Pun et al. (2006); Couvidat et al. (2012)). In the one-dimensional (1-D) VBS approach, organic compounds are categorized into logarithmically-spaced bins based on their saturation concentrations. The two-product Odum approach approximates SOA formation from the oxidation of a VOC precursor by generating two lumped semi-volatile products that can condense onto the particle phase. In the surrogate approach, the behavior of these products is influenced by surrogate molecules, chosen for their representative physicochemical properties for gas-particle partitioning.

The Hydrophobic/Hydrophilic Organic (H^2O) mechanism adopts the surrogate approach, accounting for the hydrophilic properties of SOAs and the effect of interactions between compounds on gas-particle partitioning. To represent autoxidation from monoterpenes, a simple chemical scheme, built from the measurements of Ehn et al. (2014), has been added to H^2O (Chrit et al. (2017)). Recent studies using this

mechanism have highlighted the potentially large influence of autoxidation for SOA formation over the Mediterranean (Chrit et al. (2017)) and for ultrafine particle formation over the city of Paris (Sartelet et al. (2022)).

Noticeably, the simplified mechanisms may not accurately capture the complex chemical pathways related to SOA formation. The assumptions used in simplified mechanisms may oversimplify interactions within the SOA formation process, leading to significant uncertainties in the model evaluation of the response to regulation assessments. Therefore, it is necessary to evaluate models and their responses taking into account different formation pathways, non-linear effects due to oxidation product interactions, and dependence on environmental conditions.

To address this issue, the GENerator of Reduced Organic Aerosol Mechanisms (GENOA) has been developed (Wang et al. (2022, 2023b)). GENOA generates concise, semi-explicit SOA mechanisms from detailed chemical mechanisms, effectively preserving the complexity of explicit SOA formation mechanisms within a size suitable for 3-D regional simulations. Version 2.0 of GENOA (Wang et al. (2023b)) employs a parallel reduction approach, allowing the processing of mechanisms from multiple SOA precursors.

This study aims to contribute to the understanding of the complex interplay between anthropogenic emissions, aerosol formation, and environmental conditions, supporting the development of effective strategies to reduce the negative impacts of anthropogenic emissions on SOA formation. Our approaches involve integrating semi-explicit SOA mechanisms generated by GENOA v2.0 into the 3-D CTM model CHIMERE (Menut et al. (2021)) coupled with the state-of-the-art aerosol module SSH-aerosol (Sartelet et al. (2020)). These condensed mechanisms specifically address SOA formation from monoterpene and sesquiterpene compounds, which are recognized as crucial biogenic SOA precursors (e.g., Hallquist et al. (2009); Hodzic et al. (2016)). The tropospheric degradation pathways of those compounds have been reported (e.g., Jenkin (2004); Jenkin et al. (2012); Khan et al. (2017)), providing necessary groundwork for their application in GENOA v2.0.

In addition to using GENOA-reduced mechanisms, this study employs the simplified H^2O mechanism for comparison. Details about the model and the simulation setup are provided in Section 2. SOA concentrations simulated with different SOA mechanisms are compared with measurements in Section 3.1, and their inter-comparison is presented in Section 3.2. The influence of SOA mechanisms on the simulated SOA concentration and composition in response to a NOx emission reduction scenario is explored in Section 3.3, with conclusions drawn in Section 4.

2. Methods

2.1. Model overview

3-D simulations are conducted using the CHIMERE model (Menut et al. (2021)), which is coupled to the aerosol model SSH-aerosol v1.3 (Sartelet et al. (2020)) through a splitting approach: the model first solves processes related to emissions, transport, and deposition simultaneously. Subsequently, it calculates the evolution of gas-phase concentrations resulting from chemical reactions. As a final step, CHIMERE launches SSH-aerosol to solve processes related to aerosol dynamics, such as condensation/evaporation of semi-volatile compounds and coagulation.

Within SSH-aerosol, gas-particle partitioning is computed using the thermodynamic module ISORROPIA (Nenes et al. (1998)) for inorganic aerosols and the Secondary Organic Aerosol Processor (SOAP) model (Couvidat and Sartelet (2015)) for organic aerosols. In SOAP, interactions between organic and inorganic compounds are estimated based on the molecular structure of the molecules, considering the non-ideality of aerosols. In this study, thermodynamic equilibrium is assumed for gas-particle partitioning. For particle size discretization, a sectional approach with ten sections is employed, encompassing diameters ranging from 10 nm to 10 μm.

2.2. SOA mechanism

In this study, two distinct SOA mechanisms for simulating SOA formation in the gas phase are utilized:

- The Hydrophilic/Hydrophobic Organic (H^2O) mechanism, based on experimental data (Couvidat et al. (2012); Majdi et al. (2019)). This simplified mechanism employs a surrogate approach, where key SOA precursors undergo oxidation to form several model species. Those surrogate species are characterized by attached molecular structures representing lumped aerosol species. The latest version of H^2O, as reported in Sartelet et al. (2020), includes a simplified scheme for the autoxidation of monoterpenes (Chrit et al. (2017)) and is adopted in this work.
- The GENOA-generated Biogenic Mechanism (GBM), reduced from near-explicit VOC mechanisms (i.e., MCM v3.3.1 combined with PRAM, referred to as the 'Ref.' mechanism). GBM is trained by the GENOA v2.0 algorithm, preserving essential reaction pathways and surrogate species crucial for biogenic SOA formation from monoterpenes and sesquiterpenes (Wang et al., (2023b)).

Table 1 offers an overview of the three SOA mechanisms discussed (i.e., H^2O, GBM, Ref.) for monoterpene (MT) and sesquiterpene (SQT) SOA formation. Although the GBM mechanism is more complex than H^2O, it remains more computationally manageable than the Ref. mechanism, from which GBM is derived. This indicates that GBM achieves a practical compromise between detailed chemical representation and computational efficiency for 3-D simulations.

For MT SOA formation, the H^2O mechanism utilizes a simple scheme with 22 reactions and 15 species, including 6 condensable organics. The GBM mechanism offers a more comprehensive framework with 197 reactions and 110 species, 23 of which are condensables. Compared to the Ref. mechanism, GBM is considerably more compact, representing only 8 % of the Ref. mechanism's size. Despite this reduction, GBM maintains high accuracy, with only a minor average reduction error of 3 % in SOA concentration, as reported by Wang et al. (2023b).

Regarding SQT SOA formation, H^2O adopts a highly simplified scheme of three reactions and three species (two condensables). This scheme is based on the first-generation degradation of SQT, excluding RO_2 reactions and the direct effects of inorganic radicals on SQT SOA formation. In contrast, the GBM mechanism provides a more detailed representation of SQT SOA formation. It encompasses 23 reactions and 17 species (6 condensables), representing only 2 % of the Ref. mechanism with a small average reduction error of 3 %. GBM also accounts for the direct influences of inorganics by incorporating five reactions with NO and three with HO_2. The reaction pathways related to SQT SOA formation can be found in the Supplement material Eq. S1 for H^2O and Fig. S3 for GBM.

2.2.1. Monoterpene HOM formation

MT SOA species can be classified as either HOM or non-HOM species, where HOM species are those ELVOCs formed through RO_2 reactions and autoxidation (Bianchi et al. (2019)). Fig. 1 illustrates the pathways for HOM formation in the H^2O and GBM mechanisms. Details on the

Table 1
Size of schemes for MT and SQT SOA formation in different SOA mechanisms.

Precursor	Monoterpene (MT)			Sesquiterpene (SQT)		
Mechanism	H^2O	GBM	Ref.	H^2O	GBM	Ref.
Reaction	22	197	3001	3	23	1625
Species	15	110	1227	3	17	579
Condensable	6	23	975	2	6	365
RO_2	5	44	234	0	5	112

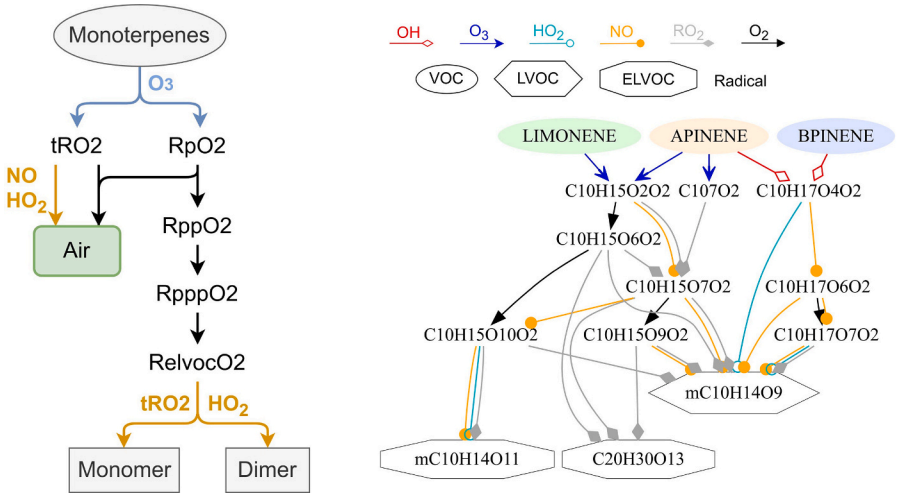

(a) H^2O (b) GBM

Fig. 1. Formation pathways of HOM species from MT oxidation in (a) H^2O and (b) GBM mechanisms.

reaction pathways for non-HOM MT condensables and the comprehensive aerosol properties of all condensables are available in the supplemental materials, specifically within S1.1 and S1.4.

In the H^2O mechanism, HOM formation is processed by five RO_2 species (i.e., tRO2, RpO2, RppO2, RpppO2, RelvocO2) that undergo multi-generation autoxidation, leading to two hydrophobic HOM condensables (i.e., Monomer and Dimer), representing all C_{10} and C_{20} MT SOA species. Notably in H^2O, RO_2 reactions with inorganics (i.e., NO and HO_2) and another RO_2 are considered for HOM formation in a simplified way (with one or two reactions), while it is not included for non-HOM formation.

In the GBM mechanism, HOM formation is more complex than those in H^2O. Reduced from the PRAM mechanism, GBM contains 32 reactions and 12 species derived from ozonolysis of α-pinene and limonene as well as OH-initiated reactions from α-pinene and β-pinene. These pathways result in nine HOM RO_2 species, which, through subsequent RO_2 reactions and autoxidation, lead to three HOM condensables: two C_{10} monomers (i.e., mC10H14O11 and mC10H14O9) and one C_{20} dimer (i.e., C20H30O13). Meanwhile, GBM comprehensively accounts for the influence of inorganic radicals on MT SOA formation. It includes 48 RO_2 reactions with NO (seven for HOMs), 36 with HO_2 (three for HOMs), and eight acyl peroxy radical (RCO_3) reactions with NO_2. The MT RO_2 pool in GBM comprises 19 species, contributing to 25 RO_2-RO_2 reactions.

2.2.2. Adjustment for 3-D simulations

In the 3-D simulations using the H^2O mechanism, the parameterization of Pun and Seigneur (2007) is typically used to account for intraparticle reactions over acidic particles, such as oligomerization. This enhances the partitioning of compounds like pinonaldehyde. For example, Lemaire et al. (2016) demonstrated that SOA formed via this parameterization could account for up to 50 % of the total biogenic SOA concentrations. While theoretically possible, the reactive uptake of pinonaldehyde onto an acidic particle was shown to be too slow to be significant under atmospheric conditions (Couvidat et al. (2018b)). In this study, simulations with H^2O are conducted both with and without the activation of this parameterization to assess its influence. Further adjustments to the SOA mechanism for integration into 3-D simulations are detailed in Supplemental Material S1.3.

2.3. Simulation configuration

Simulations are performed over Europe (latitudes from 32°N to 70°N and longitude from 17°W to 39.8°E), with a horizontal resolution of 0.25° × 0.4°. The organic aerosol (OA) concentrations and compositions from 1 June to 31 August 2018 are investigated, considering that biogenic aerosol formation is expected to be significant during the summer. All simulations start 15 days before (on 15 May) to minimize the influence of initial conditions. Boundary conditions are taken from CAMS CIFS global model simulations (Flentje et al. (2021)). Meteorology is obtained from the operational analysis of the Integrated Forecasting System (IFS) model of the European Centre for Medium-Range Weather Forecasts (ECMWF) (Flentje et al. (2021)). The anthropogenic emissions of gas and particles are taken from the CAMS-REG-AP inventory (version v5.1_REF2.1) (Kuenen et al. 2022).

2.4. Biogenic emission

Biogenic emissions are estimated with the MEGAN2.1 algorithm (Guenther et al. (2012)) as implemented in CHIMERE (Couvidat et al. (2018a); Menut et al. (2021)). However, recent studies have highlighted significant uncertainties in the estimation of biogenic emissions. Globally, these uncertainties can reach a factor of two to three, with potentially even higher discrepancies at regional levels (Messina et al. (2016); Sindelarova et al. (2022)). Specifically, it is reported that biogenic emissions computed with MEGAN2.1 over Europe might significantly overestimate isoprene by approximately a factor of three, while underestimating emissions of MT by a similar factor (Jiang et al. (2019); Ciccioli et al. (2023)). With higher MT emissions, Jiang et al. (2019) shows improved model performance in simulated SOA concentrations.

Therefore, in this study, simulations are conducted using either the default MEGAN2.1 emissions or with adjusted emissions: MT and SQT emissions increased by a factor of three, and isoprene emissions decreased by a factor of three. Although the extent of emission underestimation may vary spatially and temporally, the use of these factors should provide a reasonable estimation of the uncertainties related to biogenic emissions.

2.5. Observation

The observation data are extracted from the EBAS database (https://ebas.nilu.no/, last access: 2023/01/01). As this study focuses on the organic aerosol formation, the comparisons with observations concentrate on available data for particle mass concentrations, including particles with a diameter less than 2.5 $\mu m/g$ ($PM_{2.5}$), particles with a diameter less than 10 $\mu m/g$ (PM_{10}), organic carbon mass in particles with a diameter less than 2.5 $\mu m/g$ ($OC_{PM_{2.5}}$), organic carbon mass

in particles with a diameter less than 1 $\mu m/g$ (OC_{PM_1}), as well as organic mass in PM_1 (OM_{PM_1}).

Statistical indicators, including Mean Fractional Errors (MFE) and Mean Fractional Bias (MFB), are adopted for analysis. MFE and MFB are calculated by Eqs. (1) and (2), respectively, where C_i^{mod} and C_i^{mea} are the simulated and the measured concentrations of the targeted compound at time i (N is the total number of time steps). The following two criteria reported by Boylan and Russell (2006) have been used in many studies for evaluating the model performance (e.g., Sartelet et al. (2012); Chrit et al. (2017); Couvidat et al. (2018a); Lannuque et al. (2020)): Acceptable model performance is indicated when MFE and MFB are within the ranges of 75 % and ± 60 %, respectively. The performance is considered close to optimal when MFE and MFB fall within the ranges of 50 % and ± 30 %.

$$MFE = \frac{1}{N}\sum_{i=1}^{N}\frac{2\left|C_i^{mod} - C_i^{mea}\right|}{C_i^{mod} + C_i^{mea}} \quad (1)$$

$$MFB = \frac{1}{N}\sum_{i=1}^{N}\frac{2\left(C_i^{mod} - C_i^{mea}\right)}{C_i^{mod} + C_i^{mea}} \quad (2)$$

3. Results and discussions

3.1. Comparison between simulated and measured concentrations

To evaluate different SOA mechanism settings and identify the most reliable configurations, six simulations are carried out with the H^2O and GBM mechanisms, considering or not the modified biogenic emissions and oligomerization. Below are the differences between these simulations, along with their corresponding labels used in the analysis:

- 'GBM': Simulation with the GBM mechanism.
- 'GBM-bio3': Simulation with the GBM mechanism and modified biogenic emissions (i.e., triple for MT and SQT emissions, and one-third for isoprene).
- 'H^2O': Simulation with the H^2O mechanism.
- 'H^2O-oligo': Simulation with the H^2O mechanism and activated oligomerization for monoterpene oxidation.
- 'H^2O-bio3': Simulation with the H^2O mechanism and modified biogenic emissions.
- 'H^2O-oligo-bio3': Simulation with the H^2O mechanism, activated oligomerization, and modified biogenic emissions.

Fig. 2 presents the comparisons between simulation results and the measurements in terms of MFE (Fig. 2a) and MFB (Fig. 2b) for concentrations of PM_{10}, $PM_{2.5}$, $OC_{PM_{2.5}}$, OC_{PM_1}, and OM_{PM_1}. While data for $OC_{PM_{2.5}}$ are available from 25 stations, only two stations with reliable data are found for OC_{PM_1} and OM_{PM_1} over Europe for the simulation period. For OM_{PM_1}, four stations are initially found. However, two stations are not taken into account as they introduce significant uncertainties in the comparison: one is the Puy de Dôme observatory station in France (EMEP station code: FR0030R) on top of an extinct volcano at 1471 m. This station is excluded due to its substantial altitude difference from the corresponding cell in the CHIMERE grid (average altitude at 16.9 m), indicating the model resolution is insufficient to capture the local topography of this station. The other station near Lille is the only available urban station (EMEP station code: FR0027U). It is also excluded as its urban setting necessitates a higher resolution for an accurate comparison.

According to MFB values, aerosol concentrations are underestimated in all simulations with non-modified biogenic emissions (i.e., simulations of GBM, H^2O, and H^2O-olig). Meanwhile, simulations with modified biogenic emissions, namely those of GBM-bio3 and H^2O-bio3, lead to concentrations much closer to the measurements. This is consistent with the results of Jiang et al. (2019); Ciccioli et al. (2023), indicating that underestimations on simulated SOA concentrations could be a result of the underestimation of biogenic emissions by MEGAN2.1, as previously discussed in Section 2.4.

With non-modified biogenic emissions and the H^2O mechanism, the concentrations simulated with oligomerization (H^2O-olig) are closer to measurements than those simulated with H^2O. For example, the MFE is reduced from 0.99 in H^2O to 0.63 in H^2O-olig for OM_{PM_1} while the MFB is reduced from −0.72 to −0.20 for OC_{PM_1}. However, results suggest that this parameterization artificially increases the SOA mass and compensates for uncertainties induced by biogenic emissions. For instance, the performance of H^2O-olig (MFB = −0.73, MFE = 1.07 on $OC_{PM_{2.5}}$) is lower than the performance of H^2O (MFB = −1.12, MFE = 1.21, on $OC_{PM_{2.5}}$). When accounted for the modified biogenic emission, H^2O-olig-bio3 leads to a clear overestimation of concentrations (MFB = 0.18, MFE = 0.92, on $OC_{PM_{2.5}}$).

As shown in Fig. 2, the simulations using GBM-bio3 and H^2O-bio3 outperform other simulations in terms of accuracy. These two simulations have MFE and MFB mostly in acceptable ranges for particulate concentrations except for $OC_{PM_{2.5}}$. In this case, H^2O-bio3 has an MFE of 83 %, exceeding the acceptable threshold of 75 % defined by Boylan and Russell (2006). Additional statistical indicators, such as correlation and root mean square error (RMSE) for the GBM-bio3 and H^2O-bio3 simulations, are detailed in the supplemental material S2. These indicators further indicate the better performance of the GBM-bio3 simulation, displaying higher correlation and lower RMSE compared to the H^2O-bio3 simulation.

Overall, the statistical analysis shows that the concentrations simulated with the GBM mechanism (i.e., GBM, GBM-bio3) are closer to the

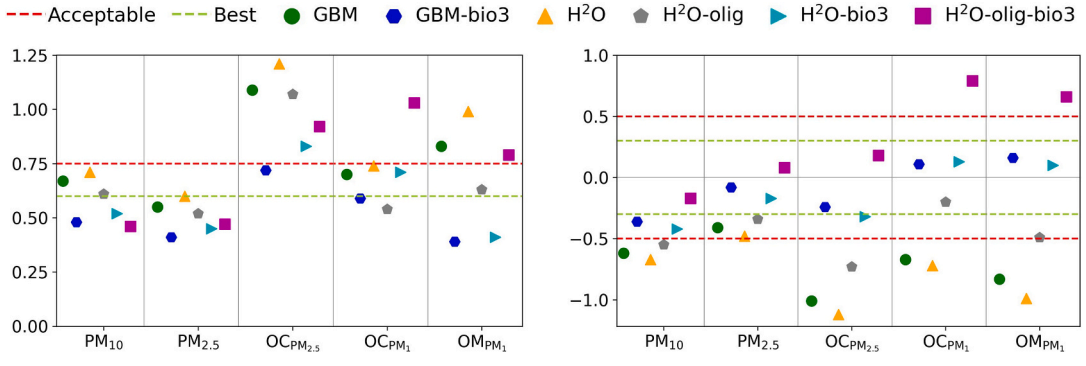

(a) MFE (b) MFB

Fig. 2. (a) MFE and (b) MFB of the different investigated simulations compared to measurements for concentrations of PM_{10}, $PM_{2.5}$, $OC_{PM_{2.5}}$, OC_{PM_1}, and OM_{PM_1} concentrations. 'Acceptable' and 'Best' lines denote the acceptable and optimal model performance ranges as reported by Boylan and Russell (2006).

measurement (with lower MFE and MFB values) than those simulated with the H^2O mechanism (i.e., H^2O, H^2O-bio3). The results indicate that using the detailed SOA mechanism such as GBM may improve the performance of SOA simulation in current 3-D modeling. Considering all results, along with the fact that the parameterization of Pun and Seigneur (2007) for oligomerization may lead to an overestimation of pinonaldehyde condensation, the GBM-bio3 and H^2O-bio3 configurations are deemed most reliable. Consequently, these configurations are utilized for the inter-comparison analysis in the subsequent sections.

3.2. Comparison between different SOA mechanisms

The 3-D results simulated using the GBM and H^2O mechanisms with modified biogenic emissions are compared in this section. For simplicity, the simulations are referred to by their SOA mechanism name, i.e., GBM for GBM-bio3 and H^2O for H^2O-bio3, in the following discussion. As no noticeable differences are observed in the concentrations of oxidants and inorganic gas-phase and particle pollutants simulated with the two mechanisms, the comparison between the two simulations focuses mainly on organic particles. The average concentrations over the simulation period of different types of organic aerosols and ratios simulated with GBM and H^2O are discussed.

3.2.1. Comparison of organic aerosol concentrations

Fig. 3a presents the map distribution of OA concentrations simulated with GBM, while the absolute concentration differences between GBM and H^2O simulations are shown in Fig. 3b. The average OA concentration over the domain simulated with the GBM mechanism is 2.2 $\mu g/m^3$ (maximum of 16.4 $\mu g/m^3$), while it is 1.7 $\mu g/m^3$ (maximum of 17.3 $\mu g/m^3$) with the H^2O mechanism. High OA concentrations ($\geq$ 5 $\mu g/m^3$) are simulated over Central Europe between 35°N and 50°N, and in Northern Europe, between 55°N to 65°N, while extreme high OA concentrations above 10 $\mu g/m^3$ are simulated in the western Balkan Peninsula, near Bosnia. Those areas correspond to areas of high biogenic emissions.

Higher OA concentrations are simulated over most continental areas of Europe using GBM compared to H^2O, with an average difference of 0.5 $\mu g/m^3$. This is particularly noticeable over Eastern Europe, Southern Spain, and north of the Mediterranean Sea. The greatest increase is simulated near the Baltic Sea, reaching up to 1.6 $\mu g/m^3$. However, in some specific areas of Central Europe where OA concentrations are high, the SOA concentrations simulated with H^2O are higher than those with GBM, with a difference of up to 2.7 $\mu g/m^3$ near Bosnia.

The results suggest that biogenic SOAs, particularly those from MTs and SQTs, dominate the total OA concentrations over Europe during the 2018 summertime for both simulations. This is consistent with several studies demonstrating the dominance of biogenic proportions in SOA concentrations, particularly in rural and suburban areas (e.g., Kelly et al. (2018); Hong et al. (2022)). Detailed information on the spatial distribution patterns of MT, SQT, and other SOAs, as well as the composition of MT and SQT SOAs, and a further discussion of the regional disparities simulated using the two mechanisms, is available in Supplemental Material S3.

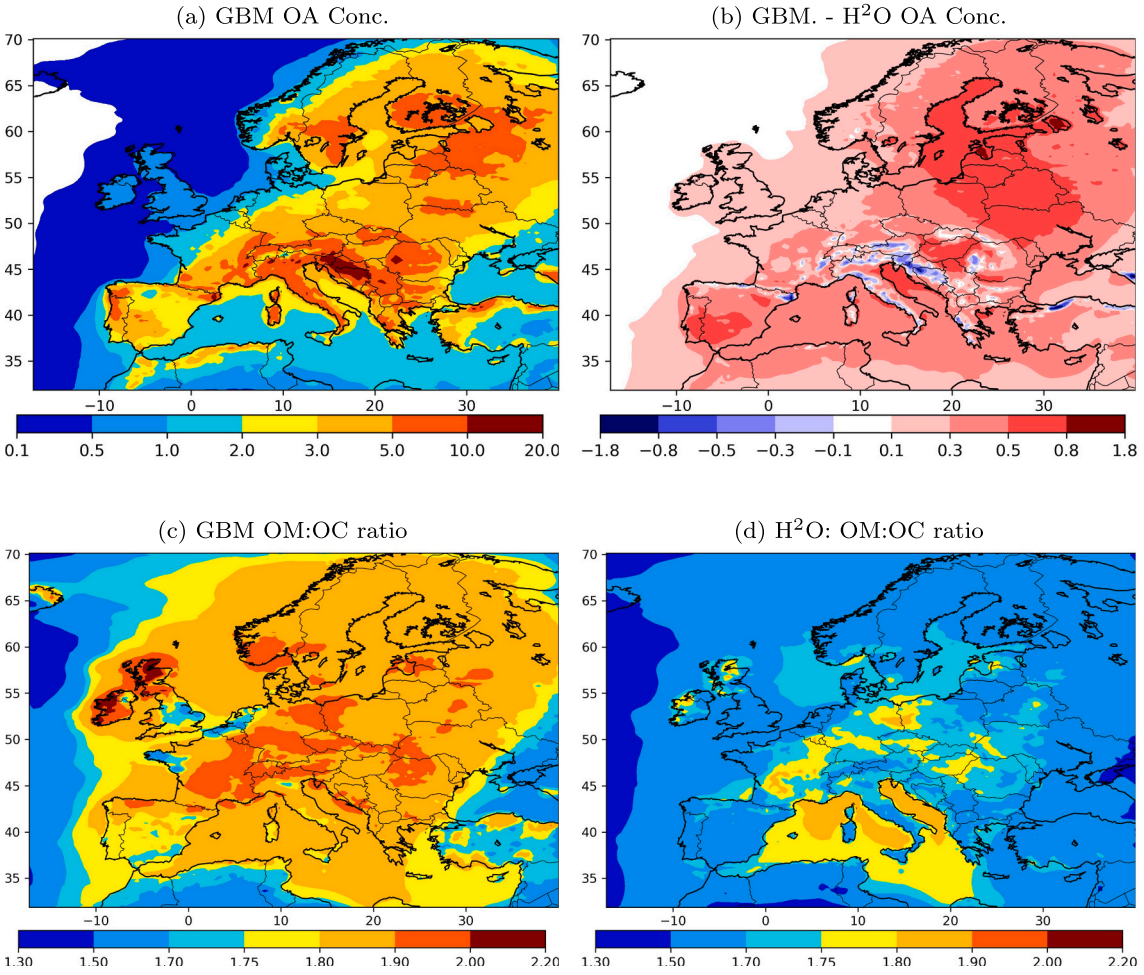

Fig. 3. Map distributions of (a) average organic aerosol concentrations simulated with GBM, (b) concentration differences between GBM and H^2O, organic mass to organic carbon (OM:OC) ratios simulated with (c) GBM and (d) H^2O.

3.2.2. Comparison of OM:OC ratios

The map distributions of organic mass to organic carbon (OM:OC) ratio simulated with both GBM and H^2O mechanisms are presented in Fig. 3c and d. A higher OM:OC ratio is simulated with the GBM mechanism with an average of 1.79 (ranging from 1.34 to 2.13), compared to the ratio simulated with H^2O with an average of 1.64 (ranging from 1.32 to 1.85). This distribution indicates that more oxidized products are simulated with GBM than with H^2O, which is consistent with the reaction pathways as more oxidized organics derived from high-generation oxidation for SOA aging are included in GBM.

However, due to the limited amount of reported data on the OM:OC ratio, determining the most realistic simulated ratios is challenging. Turpin and Lim (2001) reported a ratio of 2.1 at rural sites in the US. In Europe, Poulain et al. (2011) reported an OM:OC ratio of 1.75 at Melpitz, eastern Germany, during the summer of 2008. At the same location, the GBM and H^2O mechanisms simulated ratios of 1.91 and 1.75, respectively, suggesting a potential overestimation by the GBM mechanism. However, CHARMEX summertime measurements in the Mediterranean indicate ratios of 2.34 at Ersa in Corsica and 1.97 at Mallorca in the summer of 2013 (Chrit et al. (2017); Sartelet (2022)). At these two locations, the OM:OC ratio seems to be underestimated by both GBM (1.88 at Ersa and 1.80 at Mallorca) and H^2O mechanisms (1.69 at both Ersa and Mallorca), with a stronger underestimation by H^2O.

3.2.3. Comparison of HOM and non-HOM concentrations

Fig. 4 presents the distributions of MT SOA concentrations (both non-HOM and HOM) simulated with GBM, and the absolute concentration differences between concentrations simulated with GBM and H^2O. Overall, HOMs dominate the total MT SOAs, accounting for 64 % (0.61 $\mu g/m^3$ on average) simulated with GBM, and even much larger when simulated with H^2O, accounting for 93 % (0.68 $\mu g/m^3$). The highest concentrations of HOMs reach up to 4.4 $\mu g/m^3$ with GBM and 7.7 $\mu g/m^3$ with H^2O, whereas for non-HOMs, they peak in Central Europe at 3.2 $\mu g/m^3$ and 1.2 $\mu g/m^3$ with GBM and H^2O, respectively.

As mentioned in Section 2.2, both GBM and H^2O involve the formation of non-HOMs and HOMs from MTs, with the GBM mechanism containing more details than the H^2O mechanism involving multi-generation oxidation and a more complex dependency on inorganic radicals. As a result, GBM simulations indicate a diverse range of HOMs and non-HOMs SOAs, with notable contributions from specific hydroperoxides and first-generation oxidation products. With H^2O, simulations result in a more simplified composition with a distinct set of condensables. The supplemental material S3.2 provides detailed pie charts of MT and SQT SOA chemical compositions and an extended discussion on their variations simulated with both SOA mechanisms.

3.3. Response of biogenic SOA concentrations to NOx emission reduction

In this section, both the GBM and H^2O mechanisms are used to evaluate changes in SOA concentrations resulting from a 50 % reduction in anthropogenic NOx emissions (i.e., NO, NO_2, HONO) over the simulation domain. The scenarios before and after NOx emission reduction are referred to as the 'REF' and 'NOx50' scenarios, respectively. All other configuration settings remain the same as in the previous simulations.

3.3.1. Effect of NOx reduction on concentrations of oxidants and radicals

To understand the effect of reducing NOx emissions on SOA formation, it is essential to first investigate how NOx mitigation affects the levels of oxidants and radicals (i.e., O_3, NO_3, OH, NO, and HO_2). In response to a 50 % reduction in anthropogenic NOx emissions, the simulated NO concentrations show a direct reduction ranging from 1.7 % to 79.7 %, averaging 29.9 %, compared to the REF scenario (See the supplemental material Fig. S7).

Across most areas of Europe, a decrease in concentrations is noted for all oxidants, though the extent varies. However, in some areas with high-NOx emissions, oxidant concentrations decrease less or even increase. Similar changes in radical and oxidant concentrations due to NOx reduction are obtained in simulations using the GBM and H^2O

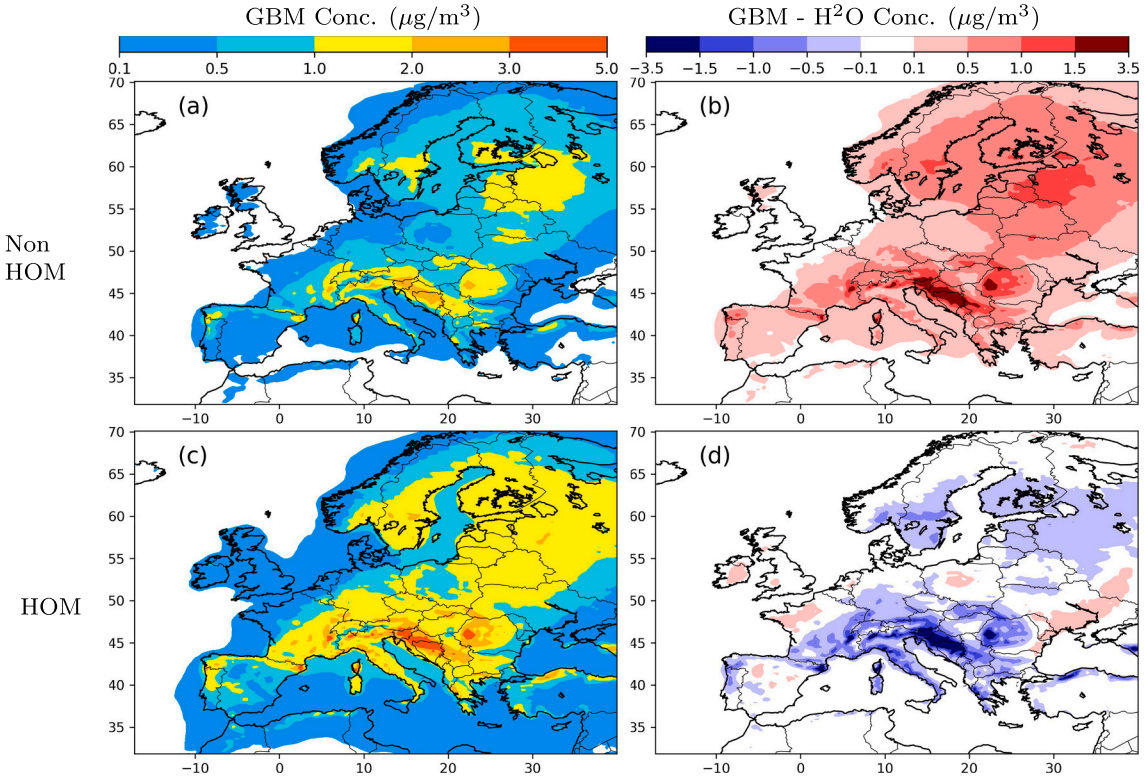

Fig. 4. Map distributions of non-HOM (top panels) and HOM (bottom panels) MT SOA concentrations simulated with the GBM mechanism (left panels) and concentration differences with the H^2O mechanism (right panels).

mechanism, as they share common inorganic reactions and VOC degradation rates. As explained by Sillman (1999), under the low-NOx regime, NOx reduction limits O_3 formation by NO_2 photolysis, leading to a decrease in O_3, NO_3, OH, and HO_2. Conversely, under the high-NOx regime, a decrease in NOx concentrations results in an antagonistic effect that increases oxidant and radical concentrations. As a result of NO and HO_2 variations, NO:HO_2 ratios decrease everywhere as a response to NOx emission reduction with an average reduction of 30.1 %. The spatial reduction in the NO:HO_2 ratio, along with more detailed data and figures illustrating changes in oxidation and radicals, is presented in the supplemental material S4.

3.3.2. Comparison of OA concentration and OM:OC ratio

In response to NOx emission reduction, the total OA concentrations increase on average over the domain by 0.07 $\mu g/m^3$ (4.5 %) when simulated with GBM and by 0.04 $\mu g/m^3$ (3.5 %) with H^2O. As displayed in Fig. 5a and b, simulations using GBM suggest that this increase can reach up to 0.66 $\mu g/m^3$ or (14.1 %) in Central Europe. Meanwhile, simulations with H^2O estimated a lower increase over mainland Europe, peaking at 0.28 $\mu g/m^3$ (11.0 %). However, some areas in Central Europe show decreases in OA concentrations, with simulated reductions down to −0.35 $\mu g/m^3$ and −0.31 $\mu g/m^3$ with GBM and H^2O, respectively.

Fig. 5c and d depicts the spatial OM:OC ratio changes due to NOx reduction as simulated with the GBM and H^2O mechanisms. Increases in OM:OC ratios are simulated with both mechanisms, averaging an absolute increase of 0.014 and 0.008 for GBM and H^2O, respectively. This trend indicates that slightly more oxidized SOAs are formed when NOx emissions are reduced, with GBM simulations showing larger increases in OM:OC ratios compared to those with H^2O. These changes in OA concentration and OM:OC ratio primarily result from variations in MT SOAs, with simulations using both mechanisms estimating an increase in MT SOA concentration across the domain due to NOx emission reduction. For spatial variations in different OAs (MT, SQT, and other SOAs) as simulated by the GBM and H^2O mechanisms, please refer to the supplemental material S4.2. The supplemental material S4.3 also includes SOA compositions under the NOx emission reduction scenario, providing additional discussion into the responses of MT and SQT SOAs.

3.3.3. Comparison of HOM and non-HOM SOAs

Fig. 6 depicts the absolute differences in MT non-HOMs and HOM concentrations between the NOx50 and REF scenarios. When dividing the total MT SOAs into non-HOM and HOM MT SOAs, it is noticeable that GBM estimates an increase in SOA concentrations for both non-HOMs (0.05 $\mu g/m^3$, amounting to a 20.8 % relative difference) and HOMs (0.03 $\mu g/m^3$ or 10.3 %) due to NOx emission reduction. Conversely, the H^2O mechanism predicts an increment in HOMs (0.04 $\mu g/m^3$ or 9.9 %) but a decrease in non-HOMs (−0.01 $\mu g/m^3$ or −2.0 %). Notably, for MT HOM concentrations, similar average increases are found with the two mechanisms but with stronger local increases with H^2O (local increases reach 0.71 $\mu g/m^3$ with H^2O against 0.47 $\mu g/m^3$ with GBM).

Those variations in concentrations can be attributed to differences in SOA mechanisms. For both non-HOM and HOM formation, the GBM mechanism preserves multi-generation oxidation, including successive bi-molecular reactions of RO_2 species with NO, HO_2, or another RO_2 species. As anthropogenic NOx emissions are reduced, NO:HO_2 ratios decrease. Since RO_2 reactions with NO and HO_2 are competitive, RO_2 reactions with HO_2 are therefore preferred, forming more hydroperoxides derived from RO_2 reactions with HO_2. Therefore, a decrease in NOx may increase MT hydroperoxide concentrations that are less volatile than other condensables, leading to more SOAs. Both Xavier et al. (2019) and Yu et al. (2021) reported similar findings, demonstrating a negative correlation between the concentration of monoterpene SOAs and NOx levels modeled with the MCM + PRAM mechanism.

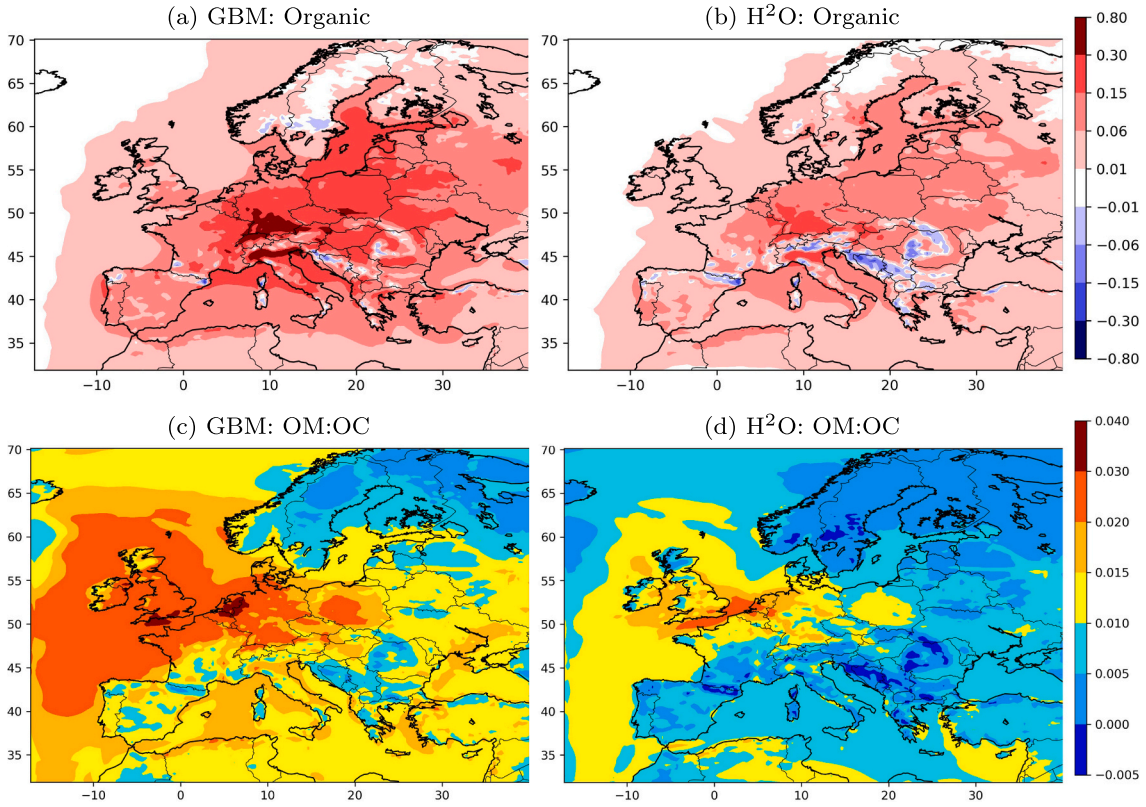

Fig. 5. Absolute differences in OA concentrations (top panels) and OM:OC ratios (bottom panels) between NOx50 and REF scenarios simulated with the GBM (left panels) and H^2O (right panels) mechanisms.

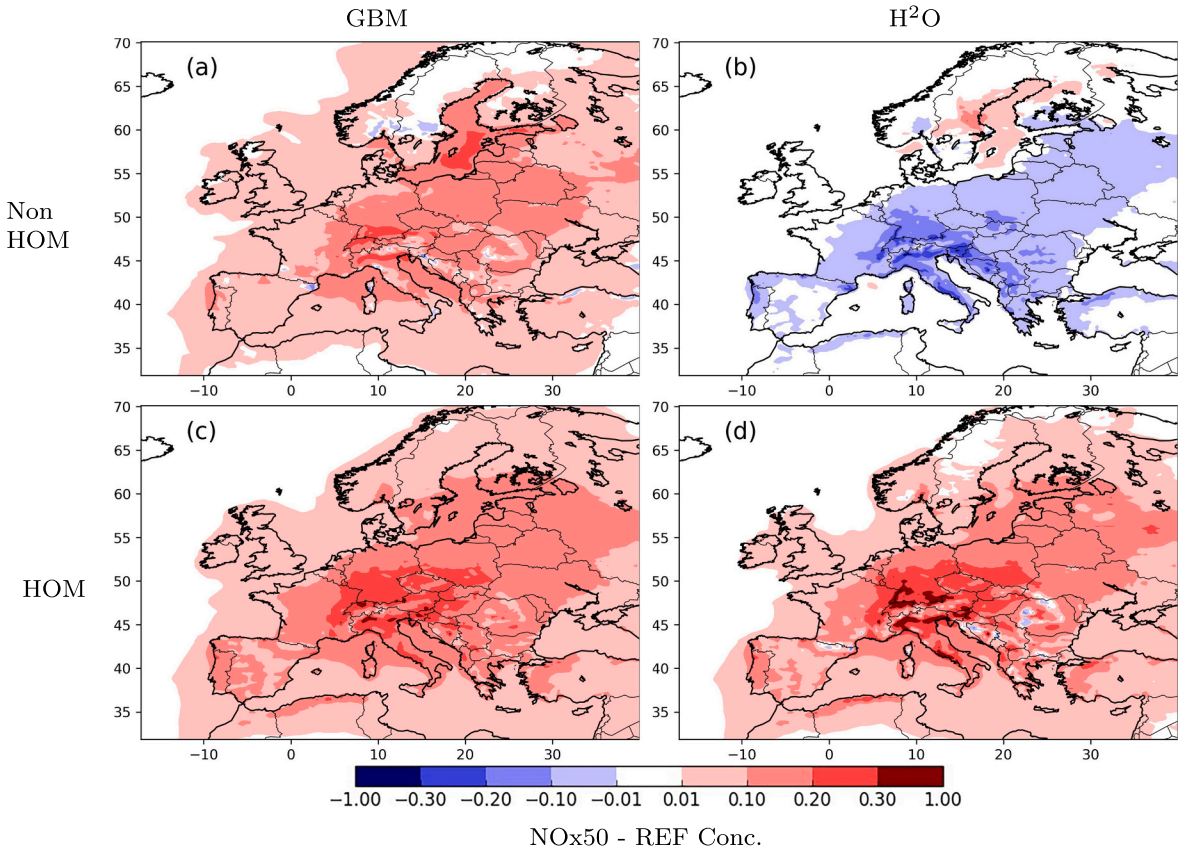

Fig. 6. Absolute differences in non-HOM (top panels) and HOM (bottom panels) MT SOA concentrations between NOx50 and REF scenarios simulated with the GBM (left panels) and H^2O (right panels) mechanisms.

Compared to GBM, H^2O contains a simple oxidation scheme for non-HOM formation which is only influenced by the degradation of precursors with the different oxidants and does not account for RO_2 reactions. As a result, the changes of NO:HO_2 ratios do not directly reflect on non-HOM concentrations. A general decrease in non-HOM SOAs is found in mainland Europe except for a small area covering part of the Baltic Sea and Sweden. This suggests that non-HOM concentration simulated with H^2O may be influenced by changes in oxidant concentrations that contribute to VOC initial degradation.

For HOM formation, the GBM mechanism preserves autoxidation and RO_2 reactions with NO, HO_2, and RO_2 that partially favor the termination of the autoxidation process. The RO_2 reactions with HO_2 and RO_2 are enhanced as a result of NOx emission reduction, which further encourages autoxidation and leads to an increase in HOM concentration. In the H^2O mechanism, the RO_2 reactions and influences of NO and HO_2 on HOM formation are also preserved but with a highly simplified scheme. As illustrated in Fig. 1, in the H^2O mechanism, NO does not directly participate in the HOM formation, it only limits autoxidation by contributing to the destruction of tRO2 species. On the contrary, HO_2 not only contributes to the destruction of tRO2 but also directly participates in the HOM formation in the H^2O mechanism via the formation of Monomer and Dimer. Therefore, when reactions with HO_2 and other RO_2 species are favorable due to NOx reduction, considerably more HOMs are produced with H^2O.

4. Conclusion

In this study, we explored the effects of anthropogenic NOx emission reduction on SOA formation through 3-D simulations employing two SOA mechanisms of varying complexity: the detailed GBM mechanism, trained from MCM and PRAM via the GENOA v2.0 reduction algorithm, and the simplified H^2O mechanism, developed from chamber experiment data. GBM is more complex than H^2O but manageable for 3-D modeling, offering detailed insights into SOA formation from MT and SQT SOA precursors, including MT HOM formation.

The 3-D simulations are conducted with CHIMERE coupled with SSH-aerosol, running across Europe for the period of June–August 2018. Initially, SOA concentrations simulated with two SOA mechanisms and different simulation settings are compared to measurements extracted from the EBAS database. With adjusted biogenic emissions obtained from MEGANv2.1, the simulations using both SOA mechanisms met the model performance standards as per Boylan and Russell (2006), underlining the need for more accurate biogenic emission calculations across Europe to minimize uncertainties. Simulations using GBM also showed better model performance in aerosol concentrations compared to those with the H^2O mechanism when benchmarked against measurements, indicating that incorporating more detailed SOA mechanisms in 3-D air quality models could further improve the accuracy of simulated SOA concentrations.

Afterward, an intra-comparison was conducted on simulations employing modified biogenic emissions with the GBM and H^2O mechanisms. Biogenic SOA, predominantly constituted by MT and SQT SOAs, are the primary contributors to OA concentrations, with high SOA levels found in Central Europe. The simulations with the GBM mechanism resulted in more oxidized OAs and higher concentrations compared to those with H^2O, because GBM contains more detailed pathways for SOA formation and aging, accounting for high-generation oxidation products from MT and SQT degradation.

Finally, the study investigated the impact of a 50 % reduction in NOx emissions on SOA formation. Both GBM and H^2O mechanisms predicted similar decreases in the NO:HO_2 ratios, particularly under high-NOx regimes, as well as an increase in SOA concentrations and oxidation

states mainly contributed by MT SOAs. Specifically, simulations with GBM predicted increases in both non-HOM and HOM concentrations for MT SOA as a response to NOx emission reduction, in contrast to simulations with H^2O, which indicated increased HOM but decreased non-HOM concentrations. This difference arises because GBM contains detailed RO_2 reactions that can respond to varying NO:HO_2 ratios, affecting both HOM and non-HOM formation that form more oxidized SOAs from $RO_2 + HO_2$ pathways when NO:HO_2 ratios decrease. H^2O, with a simple chemical scheme with no RO_2 reactions for non-HOM formation, lacks the complexity to simulate accurate non-HOM responses. Regarding SQT SOA formation, results suggest that SQT SOA formation is less sensitive to NOx mitigation compared to those of MT SOA formation.

Overall, the 3-D results indicate that detailed SOA mechanisms, such as GBM that include autoxidation, are able to capture a broader range of atmospheric chemical processes related to SOA formation and, therefore, have reliable SOA responses to environmental scenarios such as NOx emission reduction. It could be a middle ground between the computationally intensive near-explicit VOC mechanisms (e.g., MCM) and the simplified mechanism (e.g., H^2O). As a result, our study provides insights into the complexity of gas-phase chemistry on SOA formation and the importance of incorporating semi-explicit SOA mechanisms in CTMs to enhance the accuracy of air quality simulations.

CRediT authorship contribution statement

Zhizhao Wang: Writing – review & editing, Writing – original draft, Visualization, Validation, Supervision, Software, Resources, Project administration, Methodology, Investigation, Formal analysis, Data curation, Conceptualization. **Florian Couvidat:** Writing – review & editing, Supervision, Software, Resources, Project administration, Methodology, Funding acquisition, Conceptualization. **Karine Sartelet:** Writing – review & editing, Supervision, Resources, Project administration, Methodology, Funding acquisition, Conceptualization.

Declaration of competing interest

The authors declare that they have no known competing financial interests or personal relationships that could have appeared to influence the work reported in this paper.

Data availability

Data will be made available on request.

Acknowledgement

This work is financially supported by INERIS and DIM QI^2 (Air Quality Research Network on air quality in the Île-de-France region). The authors would also like to thank Dr. Marie Camredon for her valuable suggestions in improving this article.

Appendix A. Supplementary data

Supplementary data to this article can be found online at https://doi.org/10.1016/j.scitotenv.2024.172142.

References

André, M., Sartelet, K., Moukhtar, S., André, J., Redaelli, M., 2020. Diesel, petrol or electric vehicles: what choices to improve urban air quality in the Ile-de-France region? A simulation platform and case study. Atmos. Environ. 241, 117752 https://doi.org/10.1016/j.atmosenv.2020.117752.

Aumont, B., Valorso, R., Mouchel-Vallon, C., Camredon, M., Lee-Taylor, J., Madronich, S., 2012. Modeling SOA formation from the oxidation of intermediate volatility n-alkanes. Atmos. Chem. Phys. 12, 7577–7589. URL: https://acp.copernicus.org/articles/12/7577/2012/ https://doi.org/10.5194/acp-12-7577-2012.

Bianchi, F., Kurtén, T., Riva, M., Mohr, C., Rissanen, M.P., Roldin, P., Berndt, T., Crounse, J.D., Wennberg, P.O., Mentel, T.F., Wildt, J., Junninen, H., Jokinen, T., Kulmala, M., Worsnop, D.R., Thornton, J.A., Donahue, N., Kjaergaard, H.G., Ehn, M., 2019. Highly oxygenated organic molecules (HOM) from gas-phase autoxidation involving Peroxy radicals: a key contributor to atmospheric aerosol. Chem. Rev. 119, 3472–3509. https://doi.org/10.1021/acs.chemrev.8b00395.

Boylan, J.W., Russell, A.G., 2006. PM and light extinction model performance metrics, goals, and criteria for three-dimensional air quality models. Atmos. Environ. 40, 4946–4959. URL: https://www.sciencedirect.com/science/article/pii/S1352231006000690 https://doi.org/10.1016/j.atmosenv.2005.09.087.

Breysse, P.N., Delfino, R.J., Dominici, F., Elder, A.C., Frampton, M.W., Froines, J.R., Geyh, A.S., Godleski, J.J., Gold, D.R., Hopke, P.K., et al., 2013. US EPA particulate matter research centers: summary of research results for 2005–2011. Air Qual. Atmos. Health 6, 333–355. https://doi.org/10.1007/s11869-012-0181-8.

Carter, W.P.L., Jiang, J., Orlando, J.J., Barsanti, K.C., 2023. Derivation of Atmospheric Reaction Mechanisms for Volatile Organic Compounds by the SAPRC Mechanism Generation System (MechGen). EGUsphere 2023, 1–65. URL: https://egusphere.copernicus.org/preprints/2023/egusphere-2023-2343/, doi:https://doi.org/10.5194/egusphere-2023-2343.

Chrit, M., Sartelet, K., Sciare, J., Pey, J., Marchand, N., Couvidat, F., Sellegri, K., Beekmann, M., 2017. Modelling organic aerosol concentrations and properties during ChArMEx summer campaigns of 2012 and 2013 in the western Mediterranean region. Atmos. Chem. Phys. 17, 12509–12531. https://doi.org/10.5194/acp-17-12509-2017.

Ciccioli, P., Silibello, C., Finardi, S., Pepe, N., Ciccioli, P., Rapparini, F., Neri, L., Fares, S., Brilli, F., Mircea, M., Magliulo, E., Baraldi, R., 2023. The potential impact of biogenic volatile organic compounds (BVOCs) from terrestrial vegetation on a Mediterranean area using two different emission models. Agric. For. Meteor. 328, 109255 https://doi.org/10.1016/j.agrformet.2022.109255.

Couvidat, F., Sartelet, K., 2015. The secondary organic aerosol processor (SOAP v1. 0) model: a unified model with different ranges of complexity based on the molecular surrogate approach. Geosci. Model Dev. 8, 1111–1138. https://gmd.copernicus.org/articles/8/1111/2015/gmd-8-1111-2015.pdf. https://doi.org/10.5194/gmd-8-1111-2015.

Couvidat, F., Debry, E., Sartelet, K., Seigneur, C., 2012. A hydrophilic/hydrophobic organic (H2O) aerosol model: development, evaluation and sensitivity analysis. J. Geophys. Res.-Atmos. 117. URL: https://agupubs.onlinelibrary.wiley.com/doi/pdf/10.1029/2011JD017214. https://doi.org/10.1029/2011JD017214.

Couvidat, F., Kim, Y., Sartelet, K., Seigneur, C., Marchand, N., Sciare, J., 2013. Modeling secondary organic aerosol in an urban area: application to Paris, France. Atmos. Chem. Phys. 13, 983–996. https://acp.copernicus.org/articles/13/983/2013/. https://doi.org/10.5194/acp-13-983-2013.

Couvidat, F., Bessagnet, B., Garcia-Vivanco, M., Real, E., Menut, L., Colette, A., 2018a a. Development of an inorganic and organic aerosol model (CHIMERE 2017β v1. 0): seasonal and spatial evaluation over Europe. Geosci. Model Dev. 11, 165–194. URL: https://gmd.copernicus.org/articles/11/165/2018/gmd-11-165-2018.pdf, doi:https://doi.org/10.5194/gmd-11-165-2018.

Couvidat, F., Vivanco, M.G., Bessagnet, B., 2018b b. Simulating secondary organic aerosol from anthropogenic and biogenic precursors: comparison to outdoor chamber experiments, effect of oligomerization on SOA formation and reactive uptake of aldehydes. Atmos. Chem. Phys. 18, 15743–15766. URL: https://acp.copernicus.org/articles/18/15743/2018/, doi:https://doi.org/10.5194/acp-18-15743-2018.

Donahue, N.M., Robinson, A.L., Stanier, C.O., Pandis, S.N., 2006. Coupled partitioning, dilution, and chemical aging of Semivolatile organics. Env. Sc. and Tech. 40, 2635–2643. URL: https://doi.org/10.1021/es052297c, doi:https://doi.org/10.1021/es052297c.

Ehn, M., Thornton, J.A., Kleist, E., Sipilä, M., Junninen, H., Pullinen, I., Springer, M., Rubach, F., Tillmann, R., Lee, B., et al., 2014. A large source of low-volatility secondary organic aerosol. Nature 506, 476–479. URL: https://www.nature.com/articles/nature13032 https://doi.org/10.1038/nature13032.

Flentje, H., Mattis, I., Kipling, Z., Rémy, S., Thomas, W., 2021. Evaluation of ECMWF IFS-AER (CAMS) operational forecasts during cycle 41r1–46r1 with calibrated ceilometer profiles over Germany. Geosci. Model Dev. 14, 1721–1751. https://gmd.copernicus.org/articles/14/1721/2021/. https://doi.org/10.5194/gmd-14-1721-2021.

Guenther, A.B., Jiang, X., Heald, C.L., Sakulyanontvittaya, T., Duhl, T., Emmons, L.K., Wang, X., 2012. The model of emissions of gases and aerosols from nature version 2.1 (MEGAN2.1): an extended and updated framework for modeling biogenic emissions. Geosci. Model Dev. 5, 1471–1492. https://gmd.copernicus.org/articles/5/1471/2012/. https://doi.org/10.5194/gmd-5-1471-2012.

Hallquist, M., Wenger, J.C., Baltensperger, U., Rudich, Y., Simpson, D., Claeys, M., Dommen, J., Donahue, N.M., George, C., Goldstein, A.H., Hamilton, J.F., Herrmann, H., Hoffmann, T., Iinuma, Y., Jang, M., Jenkin, M.E., Jimenez, J.L., Kiendler-Scharr, A., Maenhaut, W., McFiggans, G., Mentel, T.F., Monod, A., Prévôt, A.S.H., Seinfeld, J.H., Surratt, J.D., Szmigielski, R., Wildt, J., 2009. The formation, properties and impact of secondary organic aerosol: current and emerging issues. Atmos. Chem. Phys. 9, 5155–5236. URL: https://acp.copernicus.org/articles/9/5155/2009/ https://doi.org/10.5194/acp-9-5155-2009.

Hodzic, A., Kasibhatla, P.S., Jo, D.S., Cappa, C.D., Jimenez, J.L., Madronich, S., Park, R.J., 2016. Rethinking the global secondary organic aerosol (SOA) budget: stronger production, faster removal, shorter lifetime. Atmos. Chem. Phys. 16, 7917–7941.

https://acp.copernicus.org/articles/16/7917/2016/. https://doi.org/10.5194/acp-16-7917-2016.
Hong, Y., Xu, X., Liao, D., Liu, T., Ji, X., Xu, K., Liao, C., Wang, T., Lin, C., Chen, J., 2022. Measurement report: effects of anthropogenic emissions and environmental factors on the formation of biogenic secondary organic aerosol (BSOA) in a coastal city of southeastern China. Atmos. Chem. Phys. 22, 7827–7841.
Huang, R.J., Zhang, Y., Bozzetti, C., Ho, K.F., Cao, J.J., Han, Y., Daellenbach, K.R., Slowik, J.G., Platt, S.M., Canonaco, F., et al., 2014. High secondary aerosol contribution to particulate pollution during haze events in China. Nature 514, 218–222.
Huang, X., Ding, A., Gao, J., Zheng, B., Zhou, D., Qi, X., Tang, R., Wang, J., Ren, C., Nie, W., Chi, X., Xu, Z., Chen, L., Li, Y., Che, F., Pang, N., Wang, H., Tong, D., Qin, W., Cheng, W., Liu, W., Fu, Q., Liu, B., Chai, F., Davis, S.J., Zhang, Q., He, K., 2020. Enhanced secondary pollution offset reduction of primary emissions during COVID-19 lockdown in China. Natl. Sci. Rev. 8. URL: doi:https://doi.org/10.1093/nsr/nwaa137, doi:https://doi.org/10.1093/nsr/nwaa137.
Jenkin, M., 2004. Modelling the formation and composition of secondary organic aerosol from α-and β-pinene ozonolysis using MCM v3. Atmos. Chem. Phys. 4, 1741–1757. https://doi.org/10.5194/acp-4-1741-2004.
Jenkin, M.E., Saunders, S.M., Pilling, M.J., 1997. The tropospheric degradation of volatile organic compounds: a protocol for mechanism development. Atmos. Environ. 31, 81–104. https://www.sciencedirect.com/science/article/abs/pii/S1352231096001057. https://doi.org/10.1016/S1352-2310(96)00105-7.
Jenkin, M., Wyche, K., Evans, C., Carr, T., Monks, P., Alfarra, M., Barley, M., McFiggans, G., Young, J., Rickard, A., 2012. Development and chamber evaluation of the MCM v3. 2 degradation scheme for β-caryophyllene. Atmos. Chem. Phys. 12, 5275–5308. https://acp.copernicus.org/articles/12/5275/2012/acp-12-5275-2012.pdf. https://doi.org/10.5194/acp-12-5275-2012.
Jiang, J., Aksoyoglu, S., Ciarelli, G., Oikonomakis, E., El-Haddad, I., Canonaco, F., O'Dowd, C., Ovadnevaite, J., Minguillón, M.C., Baltensperger, U., Prévôt, A.S.H., 2019. Effects of two different biogenic emission models on modelled ozone and aerosol concentrations in Europe. Atmos. Chem. Phys. 19, 3747–3768. https://acp.copernicus.org/articles/19/3747/2019/. https://doi.org/10.5194/acp-19-3747-2019.
Kanakidou, M., Seinfeld, J., Pandis, S., Barnes, I., Dentener, F.J., Facchini, M.C., Dingenen, R.V., Ervens, B., Nenes, A., Nielsen, C., et al., 2005. Organic aerosol and global climate modelling: a review. Atmos. Chem. Phys. 5, 1053–1123. https://acp.copernicus.org/articles/5/1053/2005/acp-5-1053-2005.pdf. https://doi.org/10.5194/acp-5-1053-2005.
Kelly, J.M., Doherty, R.M., O'Connor, F.M., Mann, G.W., 2018. The impact of biogenic, anthropogenic, and biomass burning volatile organic compound emissions on regional and seasonal variations in secondary organic aerosol. Atmos. Chem. Phys. 18, 7393–7422. URL: https://acp.copernicus.org/articles/18/7393/2018/ https://doi.org/10.5194/acp-18-7393-2018.
Khan, M., Jenkin, M., Foulds, A., Derwent, R., Percival, C., Shallcross, D., 2017. A modeling study of secondary organic aerosol formation from sesquiterpenes using the STOCHEM global chemistry and transport model. J. Geophys. Res.-Atmos. 122, 4426–4439. URL: https://agupubs.onlinelibrary.wiley.com/doi/pdf/10.1002/2016JD026415 https://doi.org/10.1002/2016JD026415.
Kuenen, J., Dellaert, S., Visschedijk, A., Jalkanen, J.P., Super, I., Denier van der Gon, H., 2022. CAMS-REG-v4: a state-of-the-art high-resolution European emission inventory for air quality modelling. Earth Syst. Sci. Data 14, 491–515. https://essd.copernicus.org/articles/14/491/2022/. https://doi.org/10.5194/essd-14-491-2022.
Lannuque, V., Couvidat, F., Camredon, M., Aumont, B., Bessagnet, B., 2020. Modeling organic aerosol over Europe in summer conditions with the VBS-GECKO parameterization: sensitivity to secondary organic compound properties and IVOC (intermediate-volatility organic compound) emissions. Atmos. Chem. Phys. 20, 4905–4931. https://acp.copernicus.org/articles/20/4905/2020/. https://doi.org/10.5194/acp-20-4905-2020.
Lemaire, V., Coll, I., Couvidat, F., Mouchel-Vallon, C., Seigneur, C., Siour, G., 2016. Oligomer formation in the troposphere: from experimental knowledge to 3-D modeling. Geosci. Model Dev. 9, 1361–1382. https://gmd.copernicus.org/articles/9/1361/2016/. https://doi.org/10.5194/gmd-9-1361-2016.
Li, J., Cleveland, M., Ziemba, L.D., Griffin, R.J., Barsanti, K.C., Pankow, J.F., Ying, Q., 2015. Modeling regional secondary organic aerosol using the master chemical mechanism. Atmos. Environ. 102, 52–61. https://www.sciencedirect.com/science/article/pii/S1352231014009194. https://doi.org/10.1016/j.atmosenv.2014.11.054.
Li, J., Chen, T., Zhang, H., Jia, Y., Chu, Y., Yan, Y., Zhang, H., Ren, Y., Li, H., Hu, J., Wang, W., Chu, B., Ge, M., He, H., 2024. Nonlinear effect of NOx concentration decrease on secondary aerosol formation in the Beijing-Tianjin-Hebei region: evidence from smog chamber experiments and field observations. Sci. Total Environ. 912, 168333. https://www.sciencedirect.com/science/article/pii/S0048969723069619. https://doi.org/10.1016/j.scitotenv.2023.168333.
Majdi, M., Sartelet, K., Lanzafame, G.M., Couvidat, F., Kim, Y., Chrit, M., Turquety, S., 2019. Precursors and formation of secondary organic aerosols from wildfires in the Euro-Mediterranean region. Atmos. Chem. Phys. 19, 5543–5569. https://doi.org/10.5194/acp-19-5543-2019.
McNeill, V.F., 2017. Atmospheric aerosols: clouds, chemistry, and climate. Annual rev. Chem. Biomol. Eng. 8, 427–444. URL: https://doi.org/10.1146/annurev-chembioeng-060816-101538, doi:https://doi.org/10.1146/annurev-chembioeng-060816-101538.
Menut, L., Bessagnet, B., Briant, R., Cholakian, A., Couvidat, F., Mailler, S., Pennel, R., Siour, G., Tuccella, P., Turquety, S., Valari, M., 2021. The CHIMERE v2020r1 online chemistry-transport model. Geosci. Model Dev. 14, 6781–6811. https://gmd.copernicus.org/articles/14/6781/2021/. https://doi.org/10.5194/gmd-14-6781-2021.
Messina, P., Lathière, J., Sindelarova, K., Vuichard, N., Granier, C., Ghattas, J., Cozic, A., Hauglustaine, D.A., 2016. Global biogenic volatile organic compound emissions in the ORCHIDEE and MEGAN models and sensitivity to key parameters. Atmos. Chem. Phys. 16, 14169–14202. URL: https://acp.copernicus.org/articles/16/14169/2016/ https://doi.org/10.5194/acp-16-14169-2016.
Nenes, A., Pandis, S.N., Pilinis, C., 1998. ISORROPIA: a new thermodynamic equilibrium model for multiphase multicomponent inorganic aerosols. Aquat. Geochem. 4, 123–152. URL: https://link.springer.com/article/10.1023/A:1009604003981 https://doi.org/10.1023/A:1009604003981.
Ng, N.L., Chhabra, P.S., Chan, A.W.H., Surratt, J.D., Kroll, J.H., Kwan, A.J., McCabe, D.C., Wennberg, P.O., Sorooshian, A., Murphy, S.M., Dalleska, N.F., Flagan, R.C., Seinfeld, J.H., 2007. Effect of NO_x level on secondary organic aerosol (SOA) formation from the photooxidation of terpenes. Atmos. Chem. Phys. 7, 5159–5174. URL: https://acp.copernicus.org/articles/7/5159/2007/, doi:https://doi.org/10.5194/acp-7-5159-2007.
Odum, J.R., Hoffmann, T., Bowman, F., Collins, D., Flagan, R.C., Seinfeld, J.H., 1996. Gas/particle partitioning and secondary organic aerosol yields. Env. Sc. and Tech. 30, 2580–2585. URL: https://doi.org/10.1021/es950943+, doi:https://doi.org/10.1021/es950943+.
Porter, W.C., Jimenez, J.L., Barsanti, K.C., 2021. Quantifying atmospheric parameter ranges for ambient secondary organic aerosol formation. ACS Earth Space Chem. 5, 2380–2397. https://doi.org/10.1021/acsearthspacechem.1c00090.
Poulain, L., Spindler, G., Birmili, W., Plass-Dülmer, C., Wiedensohler, A., Herrmann, H., 2011. Seasonal and diurnal variations of particulate nitrate and organic matter at the IfT research station Melpitz. Atmos. Chem. Phys. 11, 12579–12599. URL: https://acp.copernicus.org/articles/11/12579/2011/ https://doi.org/10.5194/acp-11-12579-2011.
Pun, B.K., Seigneur, C., 2007. Investigative modeling of new pathways for secondary organic aerosol formation. Atmos. Chem. Phys. 7, 2199–2216. https://acp.copernicus.org/articles/7/2199/2007/. https://doi.org/10.5194/acp-7-2199-2007.
Pun, B.K., Seigneur, C., Lohman, K., 2006. Modeling secondary organic aerosol formation via multiphase partitioning with molecular data. Env. Sc. and Tech. 40, 4722–4731. URL: doi:https://doi.org/10.1021/es0522736, doi:https://doi.org/10.1021/es0522736.
Roldin, P., Ehn, M., Kurtén, T., Olenius, T., Rissanen, M.P., Sarnela, N., Elm, J., Rantala, P., Hao, L., Hyttinen, N., et al., 2019. The role of highly oxygenated organic molecules in the boreal aerosol-cloud-climate system. Nat. Commun. 10, 1–15. https://doi.org/10.1038/s41467-019-12338-8.
Sartelet, K., 2022. Secondary aerosol formation and their modeling. Springer International Publishing, Cham. 165–183. https://doi.org/10.1007/978-3-030-82385-6_10.
Sartelet, K., Couvidat, F., Seigneur, C., Roustan, Y., 2012. Impact of biogenic emissions on air quality over Europe and North America. Atmos. Environ. 53, 131–141. https://doi.org/10.1016/j.atmosenv.2011.10.046.
Sartelet, K., Couvidat, F., Wang, Z., Flageul, C., Kim, Y., 2020. SSH-aerosol v1. 1: a modular box model to simulate the evolution of primary and secondary aerosols. Atmosphere 11, 525. URL: https://www.mdpi.com/2073-4433/11/5/525/htm, doi:https://doi.org/10.3390/atmos11050525.
Sartelet, K., Kim, Y., Couvidat, F., Merkel, M., Petäjä, T., Sciare, J., Wiedensohler, A., 2022. Influence of emission size distribution and nucleation on number concentrations over greater Paris. Atmos. Chem. Phys. 22, 8579–8596. https://doi.org/10.5194/acp-22-8579-2022.
Seigneur, C., 2019. Air Pollution: Concepts, Theory, and Applications. Cambridge University Press.
Seinfeld, J.H., Bretherton, C., Carslaw, K.S., Coe, H., DeMott, P.J., Dunlea, E.J., Feingold, G., Ghan, S., Guenther, A.B., Kahn, R., et al., 2016. Improving our fundamental understanding of the role of aerosol-cloud interactions in the climate system. Proc. Nat. Acad. Sci. 113, 5781–5790. https://doi.org/10.1073/pnas.1514043113.
Shrivastava, M., Andreae, M., Artaxo, P., Barbosa, H., Berg, L., Brito, J., Ching, J., Easter, R., Fan, J., Fast, J., Feng, Z., Fuentes, J., Glasius, M., Goldstein, A., Alves, E., Gomes, H., Gu, D., Guenther, A., Jathar, S., Kim, S., Liu, Y., Lou, S., Martin, S., McNeill, V., Medeiros, A., de Sá, S., Shilling, J., Springston, S., Souza, R., Thornton, J., Isaacman-VanWertz, G., Yee, L., Ynoue, R., Zaveri, R., Zelenyuk, A., Zhao, C., 2019. Urban pollution greatly enhances formation of natural aerosols over the Amazon rainforest. Nat. Commun. 10, 1046. https://doi.org/10.1038/s41467-019-08909-4.
Sillman, S., 1999. The relation between ozone, NOx and hydrocarbons in urban and polluted rural environments. Atmos. Environ. 33, 1821–1845. https://www.sciencedirect.com/science/article/pii/S1352231098003458. https://doi.org/10.1016/S1352-2310(98)00345-8.
Sindelarova, K., Markova, J., Simpson, D., Huszar, P., Karlicky, J., Darras, S., Granier, C., 2022. High-resolution biogenic global emission inventory for the time period 2000–2019 for air quality modelling. Earth Syst. Sci. Data 14, 251–270. https://essd.copernicus.org/articles/14/251/2022/. https://doi.org/10.5194/essd-14-251-2022.

Takeuchi, M., Berkemeier, T., Eris, G., Ng, N., 2022. Non-linear effects of secondary organic aerosol formation and properties in multi-precursor systems. Nat. Commun. 13, 7883. https://doi.org/10.1038/s41467-022-35546-1.

Turpin, B.J., Lim, H.J., 2001. Species contributions to PM2.5 mass concentrations: revisiting common assumptions for estimating organic mass. Aerosol Sc. and Tech. 35, 602–610. https://doi.org/10.1080/02786820152051454.

Wang, N., Kostenidou, E., Donahue, N.M., Pandis, S.N., 2018. Multi-generation chemical aging of α-pinene ozonolysis products by reactions with OH. Atmos. Chem. Phys. 18, 3589–3601. URL: https://acp.copernicus.org/articles/18/3589/2018/, doi:https://doi.org/10.5194/acp-18-3589-2018.

Wang, Z., Couvidat, F., Sartelet, K., 2022. GENerator of reduced organic aerosol mechanism (GENOA v1.0): an automatic generation tool of semi-explicit mechanisms. Geosci. Model Dev. 15, 8957–8982. URL: doi:https://doi.org/10.5194/gmd-15-8957-2022,doi:10.5194/gmd-15-8957-2022.

Wang, S., Zhao, Y., Chan, A.W.H., Yao, M., Chen, Z., Abbatt, J.P.D., 2023a. a. Organic peroxides in aerosol: key reactive intermediates for multiphase processes in the atmosphere. Chem. Rev. 123, 1635–1679. https://doi.org/10.1021/acs.chemrev.2c00430.

Wang, Z., Couvidat, F., Sartelet, K., 2023b b. Implementation of a parallel reduction algorithm in the GENerator of reduced organic aerosol mechanisms (GENOA v2.0): application to multiple monoterpene aerosol precursors. J. Atmos. Sci. 174, 106248. URL: https://www.sciencedirect.com/science/article/pii/S0021850223001131, doi:https://doi.org/10.1016/j.jaerosci.2023.106248.

Xavier, C., Rusanen, A., Zhou, P., Dean, C., Pichelstorfer, L., Roldin, P., Boy, M., 2019. Aerosol mass yields of selected biogenic volatile organic compounds–a theoretical study with nearly explicit gas-phase chemistry. Atmos. Chem. Phys. 19, 13741–13758. https://acp.copernicus.org/articles/19/13741/2019/acp-19-13741-2019.pdf. https://doi.org/10.5194/acp-19-13741-2019.

Xu, L., Du, L., Tsona, N.T., Ge, M., 2021. Anthropogenic effects on biogenic secondary organic aerosol formation. Adv. Atmos. Sci. 38, 1053–1084. https://doi.org/10.1007/s00376-020-0284-3.

Yu, Z., Jang, M., Zhang, T., Madhu, A., Han, S., 2021. Simulation of monoterpene SOA formation by multiphase reactions using explicit mechanisms. ACS Earth Space Chem. 5, 1455–1467. https://doi.org/10.1021/acsearthspacechem.1c00056.